Magnesium phosphate-based cements containing Halloysite nanotubes for cracks repair

Contents lists available at ScienceDirect

Construction and Building Materials

journal homepage: http://ees.elsevier.com

Magnesium phosphate-based cements containing Halloysite nanotubes for cracks repair

Monica Tonelli [1], Rita Gelli [1], Francesca Ridi *, Piero Baglioni

Department of Chemistry "Ugo Schiff" and CSGI, University of Florence, via della Lastruccia 3, 50019 Sesto Fiorentino, Florence, Italy

ARTICLE INFO

Article history:
Received 25 February 2021
Received in revised form 4 June 2021
Accepted 20 June 2021
Available online xxx

Keywords
Magnesium phosphate cements
Halloysite nanotubes
Release kinetic
Anti-fouling
Cracks repair
Concrete infrastructures

ABSTRACT

The repair of damaged cement structures represents an important area of the construction field, with dramatic structural and economic impact. Among all the available repair materials, magnesium phosphate cements (MPCs) are commonly used for their fast setting and hardening, low shrinkage and excellent bonding to aged concrete surfaces. In this work a new material made of MPC doped with Halloysite nanotubes was developed for the repair of cement-based structures, in particular of cultural heritage interest. Halloysites were introduced in the composite for a twofold reason: *i)* to enhance the mechanical properties of MPCs; *ii)* to provide slow delivery of active molecules. Here, Halloysites were loaded with an antimicrobial agent, sodium salicylate, to achieve anti-fouling protection properties. The composites were thoroughly characterized to get a complete overview of the physico-chemical features of the repair material and to unravel the effect of the inorganic nanotubes by means of X-ray diffraction, scanning electron microscopy, FT-IR spectroscopy, thermogravimetry, porosimetry and mechanical testing. The incorporation of Halloysites in MPCs improves the handling and mechanical properties of the cements and allows for the release of active molecules from the cement matrix. Some preliminary applications of the composite were conducted in a real case study, demonstrating that it can be effectively used for crack repair and that the use of Halloysites as nano-carriers confers additional specific protection through the slow delivery of anti-fouling molecules from MPCs.

1. Introduction

Over the last decades, the use of repair materials for concrete structures became crucial, given the large number of concrete-based monuments that are prone to continuous damages. Cementitious materials are among the largest produced materials by humankind, and Portland cement is the largest used hydraulic binder for building purposes [1]. Nevertheless, the repair of deteriorated concrete structures, essential to allow their use and preservation in safe conditions, does not have a universally-recognized and developed conservation methodology [2,3]. A good repair procedure should improve the performance of the structure, restore its strength and stiffness, recover its appearance and improve its durability, also by preventing chemical and biological degradation processes [4,5]. A variety of rapid hardening materials for concrete's repair are reported in the literature, namely epoxy resins, polyester resins, polymer latex, polyvinyl acetate, various cement-based inorganic binders [4], calcium aluminate cement [6], alkali activated cement [7] and Portland cement [8,9]. Despite the compositional affinity, some of the drawbacks of classic repair materials based on neat cement include a slow hardening time, a low tensile strength and adhesion; furthermore, they are not suitable for repairing thin sections [10]. Hence, Portland or blended cements should be mixed with aggregates, fibers and other additives to achieve the required properties [11]. In the last years, magnesium phosphate cement (MPC) has received increasing attention as repair material for cementitious structures, thanks to its quick setting and hardening, low shrinkage and good bonding ability [12–15]. MPCs can be prepared through the reaction between MgO or $Mg_3(PO_4)_2$ (tri-magnesium phosphate, TMP) and a soluble phosphate salt (typically an ammonium or potassium phosphate), producing struvite ($MgNH_4PO_4{\cdot}6H_2O$) as a binding reaction product [16–18]. It is reported that MPC prepared from ammonium phosphate and MgO release ammonia during the setting, creating unpleasant odor and favoring corrosion phenomena [14,19]. The preparation of MPC through the reaction between MgO and potassium phosphate or the replacement of MgO with TMP allows avoiding this drawback [20]. MPCs result particularly suitable for applications in the rapid repair of infrastructures for multiple reasons: (1) fast setting, which is particularly useful when restoring heavy traffic areas; (2) high early strength [21–23]; (3) low dry shrinkage and no bleeding phenomena [14,24]; (4) capability to set and harden at very low tempera-

*Abbreviations*MPCMagnesium Phosphate Cement.HNTsHalloysite Nanotubes.TMPTri-Magnesium Phosphate.DAHPDi-Ammonium Hydrogen Phosphate.SASalicylate.XRDX-Rays Diffraction.PDFPowder Diffraction File.FT-IRFourier Transform-Infrared Spectroscopy.TGAThermogravimetry.SSASpecific Surface Area.PSDPore Size Distribution.BETBrunauer-Emmet-Teller.BJHBarrett-Joyner-Halenda (BJH).FE-SEMField Emission-Scanning Electron Microscopy.

* Corresponding author.
E-mail address: francesca.ridi@unifi.it (F. Ridi)

[1] These authors equally contributed to the work.

https://doi.org/10.1016/j.conbuildmat.2021.124056
0950-0618/

tures [25]; (5) high bonding strength with old concrete [14]; (6) high deicer-frost resistance and abrasion resistance [24]; (7) fire-proof behavior [26]; (8) low thermal expansion coefficient [27].

Conservation of degraded cement-based historical monuments and structures is an important issue and requires the development of compatible consolidants. New formulations enriched with inorganic admixtures as Halloysite nanotubes (HNTs), that are expected to enhance damaged structures lifetime, constitute a possible method to improve materials for conservation. HNTs are nanotubular clays compatible with cementitious materials [28,29], ideal for reinforcing purposes, abundant in many locations around the world, cheap, non-toxic and endowed with an empty lumen which can be loaded with active molecules to obtain a controlled release [30–33]. Nowadays, HNTs are used in many applications, both as nanocarriers and to increase the mechanical performances of various materials, and they were recently used also in cementitious materials made of Portland cement [28,34]. MPCs blended with pozzolanic materials, aggregates, fillers and other admixtures, such as retarders [35], are reported in the literature. Fibers addition to these composites is a well-recognized method for improving the ductility and flexural toughness of MPCs, and different types have been used in MPCs, including steel fibers [36,37], basalt fibers [38], glass fibers [26], polypropylene chopped fibers [39], and coir fibers [40]. Few studies are reported on the effect of clays and nanotubular materials on the MPCs properties: bentonite clay [41], metakaolin [42], and carbon nanotubes [43,44] were shown to improve the microstructure of MPCs and enhance their mechanical properties. Nevertheless, the inclusion of a nanotubular clay which could reinforce the MPC while simultaneously releasing an active molecule could represent an innovative approach to further improve the features of MPCs as repair materials. In this perspective, HNTs represent ideal candidates, and their inclusion in MPCs, to the best of our knowledge, was never reported so far.

In this work a new repair material for cement-based structures made of MPC doped with HNTs as nano-carriers was prepared. HNTs were loaded with an antimicrobial agent, sodium salicylate (SA) [45,46] to provide anti-fouling properties that would protect the damaged structure from the aggression of microorganisms and prevent the formation of a biofilm [47,48]. The composite was characterized to understand the effect of HNTs on the properties of the "hybrid" material, and the SA kinetic release from pristine HNTs and from the composite MPC/HNTs was analyzed. Results show that HNTs can be used as nano-reservoir for MPC repair materials providing a slow delivery of actives into MPC matrix. The composite resulted to be quickly and easily applicable, showed improved properties and prolonged the protective effect of the molecules loaded into HNT cavities, which would prevent expensive conservation procedures, reducing costs arising from periodical maintenance.

2. Materials and methods

2.1. Samples' preparation

2.1.1. Materials

Newberyite ($MgHPO_4{\cdot}3H_2O$, purity > 97%) was purchased from Sigma-Aldrich, while Magnesium hydroxide ($Mg(OH)_2$, purity > 95%) was obtained from Fluka. Di-Ammonium Hydrogen Phosphate ($(NH_4)_2HPO_4$, DAHP, purity > 99%) was supplied by Riedel de Haën. Dragonite™ Halloysite nanotubes were kindly provided by Applied Minerals Inc; according to their datasheet, HNTs have a length of 0.5–2 μm, outside diameter 50–70 nm, inner diameter 15–45 nm and a specific surface area of 65 m^2/g. Sodium salicylate (NaSA, purity 99.5%) was purchased from Sigma-Aldrich. Milli-Q water was used throughout all the experiments. All materials were used as received, without any further purification.

2.1.2. Preparation of TMP

Tri-Magnesium Phosphate (TMP) was obtained by means of a calcination reaction, following a method reported in the literature [17]. Briefly, 60 g of newberyite ($MgHPO_4{\cdot}3H_2O$) and 10 g of $Mg(OH)_2$ (molar ratio 2:1) were mixed and placed in ceramic crucibles. The powder was heated in a muffle (Nabertherm) at 1000 °C for 5 h to form $Mg_3(PO_4)_2$ according to the following reaction:

$$Mg(OH)_2 + 2MgHPO_4{\cdot}3H_2O \rightarrow Mg_3(PO_4)_2 + 8H_2O$$

After quenching at room temperature, the calcined product was crushed with agate mortar and pestle and sieved (cut-off 150 μm).

2.1.3. Preparation of MPCs with HNTs

Cements were typically prepared by mixing 0.5 g of TMP with different amounts of HNTs (0%, 2%, 5% and 10% weight HNTs/weight TMP). The two powders (TMP and HNTs) were accurately mixed with a spatula for at least 3 min to ensure a complete homogenization. The cement pastes were then prepared by adding 0.333 mL of a 3.5 M aqueous solution of DAHP, obtaining a 1.5 g/mL TMP/liquid (TMP/L) ratio (see Table 1). The cement forms according to the following reaction [17]:

$$Mg_3(PO_4)_2 + (NH_4)_2HPO_4 + 15H_2O \rightarrow 2MgNH_4PO_4{\cdot}6H_2O + MgHPO_4{\cdot}3H_2O$$

After mixing for about 30 s, pastes were poured in plastic molds with 1 cm-diameter and set at room temperature and relative humidity > 96% for at least 5 days before characterization.

2.1.4. Loading of HNT with SA

The encapsulation of SA in HNTs was performed in slightly basic aqueous solution, as reported elsewhere [46,49]. 1 g of HNTs was mixed as a dry powder in a concentrated solution of sodium salicylate in water (11 g NaSA in 12.5 mL of water), adjusting the pH of the solution at ~ 8 with NaOH 1 M to maximize the electrostatic interaction between the lumen of the nanotubes and salicylate. The suspension was then evacuated, kept under vacuum at p < 20 mbar for 3 h and cycled back to atmospheric pressure for 1 h. Afterwards, the suspension was kept again at p < 20 mbar for 1 h and cycled back to atmospheric pressure for 1 h. The cyclic in/out vacuum pumping procedure was repeated three times in total. Finally, HNTs were separated from the solution by centrifugation, washed with water to remove unbound molecules and dried overnight at 60 °C.

2.2. Characterization techniques

2.2.1. Gillmore test

The initial and final setting times of the pastes were measured by means of a Gillmore apparatus (Matest, Bergamo, Italy), according to the ASTM standard C-266. The experiment was carried out on fresh pastes, prepared according to the compositions in Table 1. Immediately after mixing, the pastes were placed in plastic molds and the surface was tested every 2 min with the Gillmore apparatus. Cement is

Table 1
Nomenclature and composition of the prepared samples.

Sample	TMP (g)	HNT (g)	DAHP 3.5 M (mL)	% wt HNT/TMP	TMP/L (g/mL)
H0	0.5	0	0.333	0	1.5
H2	0.5	0.01	0.333	2	1.5
H5	0.5	0.025	0.333	5	1.5
*H*10	0.5	0.05	0.333	10	1.5

considered to attain its initial or final setting time when its surface respectively bears the initial or final Gillmore needle without appreciable indentation ("initial setting" needle ∅ = 2.12 mm, weight 113.4 g and "final setting" needle ∅ = 1.06 mm, weight 453.6 g).

2.2.2. X-Ray diffraction (XRD)

XRD data were collected with a D8 Advance with DAVINCI design (Bruker, Milan, Italy), using as X-rays source the Cu Kα radiation (wavelength λ = 1.542 Å), at 40 kV and 40 mA, a 2θ range of 10 – 60°, a step size of 0.03° and a time/step of 0.3 s. Before the analysis, set cements were grinded with mortar and pestle and flattened on a Si zero-background sample holder. Peaks' assignment was based on the Powder Diffraction Files (PDF) of the database of the International Centre for Diffraction Data.

2.2.3. Fourier Transform-Infrared spectroscopy (FT-IR)

FT-IR spectra were collected using a Bio-Rad FTS-40 spectrophotometer (Hercules, CA, USA). The samples were analyzed in KBr pellets prepared by mixing 1.00 ± 0.05 mg of sample with 100.0 ± 0.1 mg of KBr (Sigma-Aldrich, FT-IR grade). The spectra were acquired in the range 4000 – 400 cm^{-1} using a resolution of 2 cm^{-1}, 64 scans and scan delay of 600 s.

2.2.4. Thermogravimetry (TGA)

Thermogravimetric analyses were performed by means of a STD Q600 instrument (TA Instruments, New Castle, US). Samples placed in alumina pans were measured from room temperature to 1000 °C at 10 °C/min in nitrogen flux (100 mL/min).

2.2.5. Gas porosimetry

The Specific Surface Area (SSA) and Pore Size Distribution (PSD) of the cements were determined with a Coulter SA 3100 analyzer (Beckman Coulter), using nitrogen as adsorptive gas. Set cement samples were cut into small pieces and inserted in samples' holders. Prior to the measurements, samples were outgassed for 2 h at 50 °C. The mild outgas temperature was chosen in order to prevent the conversion of struvite to different phases, such as dittmarite [50]. The specific surface area (SSA) was obtained using the Brunauer-Emmet-Teller (BET) method, while the pore size distribution was estimated using Barrett-Joyner-Halenda (BJH) analysis.

2.2.6. Field Emission-Scanning electron Microscopy (FE-SEM)

FE-SEM images were collected on cements' cross-sections with a field-emission ΣIGMA microscope (Carl Zeiss Microscopy, Germany). Specimens were fixed on aluminum stubs by means of conductive tape. The accelerating potential was 2.00 kV, with a ~ 4 mm working distance. Images were acquired using an InLens detector.

2.2.7. Compressive strength measurements

The compressive strength of the set cements was tested by performing a compression analysis with an electromechanical universal testing machine Instrom 5500 L with a 10 kN load cell. Sample H0 was prepared by mixing 2.4 g of TMP with 1.6 mL of DAHP solution 3.5 M, whereas for sample *H*10, 0.24 g of HNTs were carefully mixed with 2.4 g of TMP before the addition of DAHP solution. The pastes were poured in cylindrical molds (diameter 13 mm, height ~ 13 mm) and were set at room temperature, at relative humidity > 96% for 5 days. The specimens were extracted from the molds and polished with abrasive paper to obtain an aspect ratio of about 1 (height/diameter), making the two surfaces of the cylinders as flat as possible. Five samples were prepared for each composition, and the reported results are the average ± the associated standard deviation.

2.2.8. Release kinetic

The amount of released SA from HNTs and from HNTs incorporated in MPC was quantified by means of UV–vis spectroscopy. Samples were analyzed in cuvettes with a Cary3500 spectrophotometer (Agilent) in the 400–220 nm range, with an integration time of 0.02 s and a bandwidth of 1 nm, using water as reference. Prior to the measurement, the absorbance of NaSA was measured at 296 nm to obtain the calibration curve, A = 0.033·c – 0.013, where c is the concentration of NaSA (μg/mL). The release of SA from loaded HNTs was studied by dispersing 10 mg of HNT-SA in 5 mL of water, while stirring at 25 °C. At predetermined times, 50 μL of suspension were withdrawn and replaced with 50 μL of water. The withdrawal was diluted with 450 μL of water and analyzed by UV–vis spectroscopy to quantify the amount of released SA from the nanotubes.

The release kinetic of SA from the composite containing 10 wt% of HNT-SA into MPC was investigated using a disk of *H*10-SA (diameter ~ 0.8 cm, height ~ 0.3 cm, prepared with 300 mg of TMP, 30 mg of HNT-SA and 200 μL DAHP 3.5 M solution) directly dipped in 3.5 mL of water in a cuvette, continuously stirred at 25 °C and periodically analyzed. As a reference, a MPC containing pristine HNTs was also analyzed at 296 nm, in order to detect possible contributions due to the dissolution of the cement matrix. A quantitative evaluation of the release properties was obtained by fitting the experimental data according to the most commonly used models in the analysis of drug-release. Typically, the released amount of drug is described as the ratio between the cumulative amount of drug released at time t (M_t) and at infinite time (M_∞). Three kinetic equations were used: *i)* the Higuchi equation [51], where the fractional release (M_t/M_∞) is proportional to the square root of time

$$M_t/M_\infty = k_H \cdot t^{1/2} \quad (1)$$

where k_H is the Higuchi dissolution constant; *ii)* the Korsmeyer-Peppas equation [52–54]

$$M_t/M_\infty = k_{KP} \cdot t^{n_{KP}} \quad (2)$$

where k_{KP} accounts for the structure and geometry of the dosage form, while n_{KP} is used to characterize different systems ($n_{KP} \leq 0.5$ corresponds to a Fickian transport, $0.5 < n_{KP} < 1$ corresponds to non Fickian transport, $n_{KP} = 1$ to Case-II transport, and $n_{KP} > 1$ to super Case-II transport); *iii)* the Weibull model [55,56]

$$M_t/M_\infty = 1 - exp(-k_W \cdot t^{n_W}) \quad (3)$$

where k_W defines the time scale of the process, and n_W is used to indicate the transport mechanism ($n_W \leq 0.75$ corresponds to a Fickian transport, $0.75 < n_W < 1$ indicates a combination of Fickian diffusion and Case-II transport, $n_W > 1$ indicates a complex transport mechanism).

2.2.9. Resistance of MPC to dissolution in water

The extent of MPC dissolution when in contact with water was evaluated by analyzing samples from the release experiment after incubation in water for 1 week (*i.e.,* disks of diameter ~ 0.8 cm, height ~ 0.3 cm) in 3.5 mL of water. After the release experiment, cements were freeze-dried and the weight loss % was calculated with the following equation:

$$Weightloss\% = \frac{weightafterincubation}{weightbeforeincubation} \times 100 \quad (4)$$

The weight after incubation was corrected for the amount of released SA from the cement (about 0.02 mg). An MPC not incubated in water was also freeze-dried, and its weight compared with that prior to lyophilization, in order to correct the values for the weight loss due to

the freeze-drying process (3.4%). The obtained values are the average of 4 replicates (the reference samples + the three replicates of MPC/HNT-SA).

2.3. Application for cracks consolidation

The cement paste *H*10 was applied in a crack to test the performances of the developed material in a real application. 2 g of TMP and 0.2 g of HNTs were mixed with a spatula; after the homogenization of the powders, 1.333 mL of DAHP 3.5 M were added, and the paste was mixed for about 30 s. The fresh cement was loaded in a syringe, and extruded directly in the selected cracks, after 3 min from the beginning of the mixing.

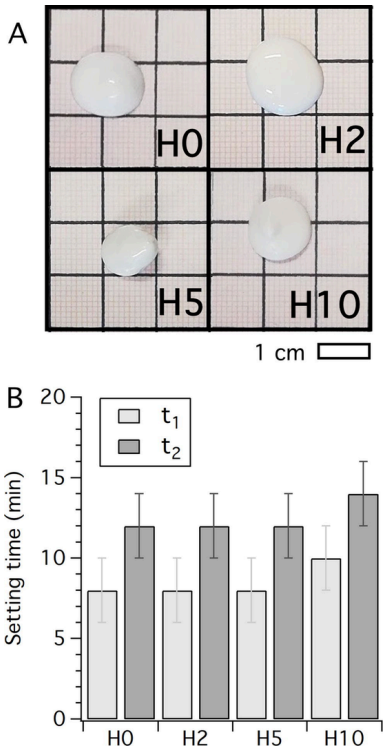

Fig. 1. (A) Photos of freshly prepared formulations poured on millimeter grid paper and (B) corresponding setting times, obtained by means of the Gillmore test. H0, H2, H5 and *H*10 refer to MPCs prepared with 0, 2, 5 and 10% of HNTs, respectively (see Table 1).

3. Results and discussion

3.1. Effect of HNTs on MPC pastes

The effect of HNTs on the consistency and fluidity of the cement pastes was initially evaluated by analyzing the aspect of the pastes poured on millimeter grid paper immediately after mixing. The results of the test, reported in Fig. 1A, reveal that HNTs increase the compactness of the paste, making it less fluid, improving the moldability and the handling properties. This effect is not related to the setting time of the cements, which is shown in Fig. 1B: all formulations achieve an initial setting time (t_1) in 8–10 min and a final setting time (t_2) in 12–14 min. Therefore, considering the experimental error associated to the Gillmore test, the setting time does not depend on HNT content. The obtained setting times are in line with other reports for MPCs [20], and demonstrate that the fast setting kinetic of these materials is not influenced by the presence of HNTs. A quick setting process is crucial for rapid repair applications, such as concrete repair [13,14,24]. It is worth mentioning that when longer setting times are required for a specific application, retarders such as borax can be easily included in the formulation [57].

3.2. Characterization of the set cements

Set cements were analyzed in order to investigate the formed phases and the microstructure, and the results are reported in Fig. 2. The crystallinity was evaluated to detect the possible effect of HNTs on the phases formed in cement formulations. XRD patterns of sample H0 and *H*10 in Fig. 2A do not show any significant difference: in both samples the diffraction peaks are attributed to struvite ($MgNH_4PO_4{\cdot}6H_2O$, PDF: 03–0240), newberyite ($MgHPO_4{\cdot}3H_2O$, PDF: 01–0597) or farringtonite ($Mg_3(PO_4)_2$, PDF: 25–1373) which are respectively the products and the reactant of the setting reaction of MPCs, reported in section 2.1.3.

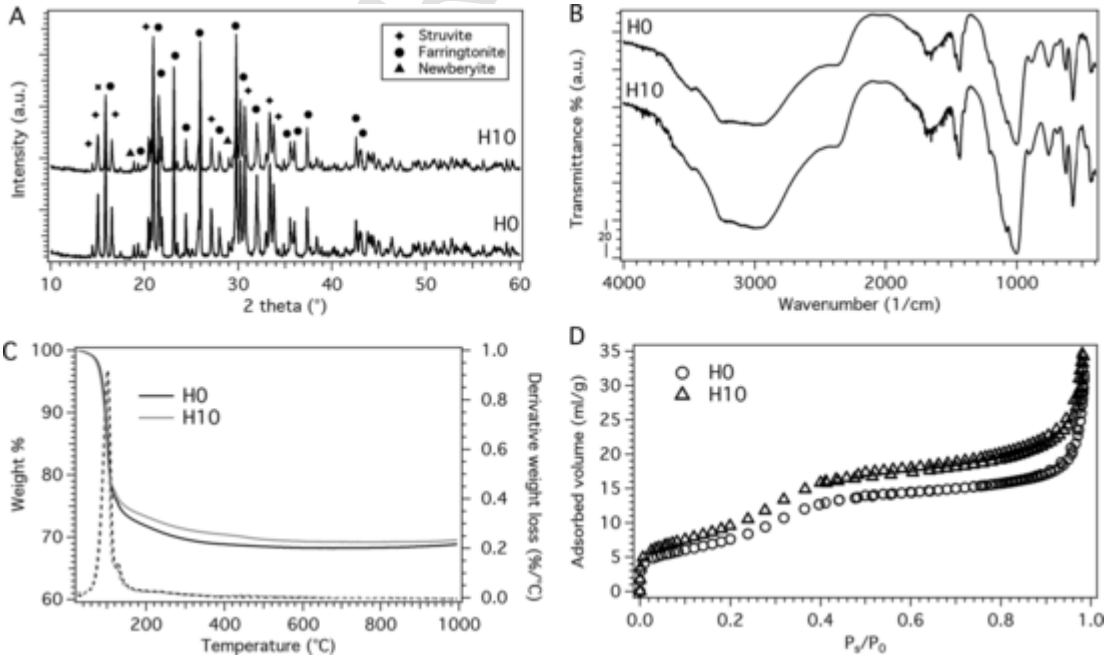

Fig. 2. (A) XRD patterns, (B) FT-IR spectra, (C) TGA curves and (D) Nitrogen adsorption/desorption isotherms of samples H0 and *H*10.

The XRD signals of HNTs are not detectable in the *H*10 sample, likely due to the very poor intensity of its diffraction peaks compared to that of the other phases (see the diffraction pattern in Figure S1A).

Samples were also analyzed by means of FT-IR spectroscopy (see Fig. 2B) and, in agreement with XRD, no differences were observed between the two samples: all peaks are related to phosphate, water or ammonium absorptions of the phases constituting the MPC matrix. The detailed peaks' assignment is reported in Table 2.

HNTs signals are not visible in *H*10 spectrum, probably due to the small quantity of nanotubes present in the formulation and to the fact that their signals are superimposed to those of the MPC phases (at about 500 cm^{-1}, 1000 cm^{-1} and 3700 cm^{-1}, see the spectrum in Figure S1B).

Further information about the phases present in the samples were obtained from thermal analysis. The thermograms of samples H0 and *H*10, reported in Fig. 1C, show that both cements lose their weight in a single step centered at about 100 °C. The weight loss at 1000 °C is 30.5% for H0 and 31.1% for *H*10: the slightly smaller weight loss of *H*10 likely accounts for the presence of HNTs in the sample, that only lose 17.1% of their weight when heated at 1000 °C (see the thermogram in Figure S3). Summarizing, the thermogravimetric curves reflect the weight loss of the hydrated phases constituting the cement matrix, *i.e.* struvite and newberyite, which upon heating gradually lose water and ammonia molecules [61,62].

Table 2
FT-IR peaks' assignment.

Peak (cm^{-1})	Vibration	Assignment	Reference
574	P-O bending	Farringtonite/Struvite/Newberyite	[58–60]
626	P-O bending	Farringtonite/Struvite/Newberyite	[58–60]
759	H_2O librations	Struvite	[60]
888	P-O(H) bending H_2O librations	Newberyite Struvite	[59,60]
1010	P-O stretching	Farringtonite/Struvite/Newberyite	[58–60]
1436	N–H bending	Struvite	[60]
1656	O–H bending (water)	Struvite/Newberyite	[59,60]
2355	O–H stretching	Struvite	[60]
2500–3500	O–H stretching N–H stretching	Struvite/Newberyite	[59,60]

Table 3
BET SSA and total pore volume of the investigated MPC/HNT composites.

Sample	SSA (m^2/g)	Total pore volume (mL/g)
H0	28.6	0.043
H2	38.8	0.051
H5	33.3	0.046
*H*10	36.4	0.055

Further information on the HNTs addition were obtained from the specific surface area and porosity of the cement matrix by means of gas porosimetry. The adsorption/desorption isotherms (see Fig. 2D and S3) are compatible with a reversible Type II isotherm with a multi-layer adsorption, as typically observed in MPCs [63]. The specific surface areas reported in Table 3 suggest that the inclusion of HNTs slightly increases the SSA of the cements, irrespectively of the amount present in the MPC. The pore size distribution of the samples (see Figure S4) was obtained with the BJH analysis and shows that the presence of HNTs in the cement matrix does not significantly affect the size of the pores that are in the 3–200 nm range. All MPCs display a broad pore size distribution, centered around 80 nm. The fact that HNTs do not markedly increase the SSA and the porosity of the MPC can be advantageous for a material to be used for crack repair. Water is the major vehicle of many harmful substances that are the main cause of the physical and chemical degradation processes affecting concrete buildings. A very porous repair material could therefore represent a threat to the preservation of the structural integrity of the damaged area.

Summarizing, the physico-chemical characterization of the cements reveals that HNTs do not affect the phases formed in the cement matrix nor its microstructure.

HNTs aggregate under the influence of van der Waals forces [33] into agglomerates of tens of μm [64]; therefore, to assess the formation of HNT clusters in the composites, we analyzed the samples by means of FE-SEM. Fig. 3 reports the FE-SEM of H0 and *H*10 samples. Sample H0 shows the presence of struvite crystals with the characteristic parallelepiped-like structures with cross-shaped and y-shaped cracks [65]. TMP, on the other hand, is characterized by smooth micrometric objects. *H*10 sample appears more heterogeneous than H0 and it is possible to recognize both struvite crystals and HNTs (SEM images of pristine HNT nanotubes are also reported in Figure S5 in the Supplementary Material). The nanotubes appear well dispersed into the cement matrix and no segregation was observed.

Fig. 4 reports the compressive strength of H0 and *H*10. *H*10 displays an improved compressive strength with respect to H0, showing that HNTs reinforce MPC, enhancing its load withstanding. In the literature, HNTs are widely used to increase the mechanical performances of various materials, including some cements [5,28,34] but, to the best of our knowledge, their use in MPC cements is reported here for the first time. In cements based on calcium silicate hydrate, the reinforcing effect of HNTs has been attributed to multiple mechanisms [28]: *i)* filling of cement voids; *ii)* cross-linking of the matrix by interaction of –OH groups from HNTs and Ca^{2+} in cement pastes; *iii)* interaction of silica from HNTs' surface with calcium hydroxides; *iv)*

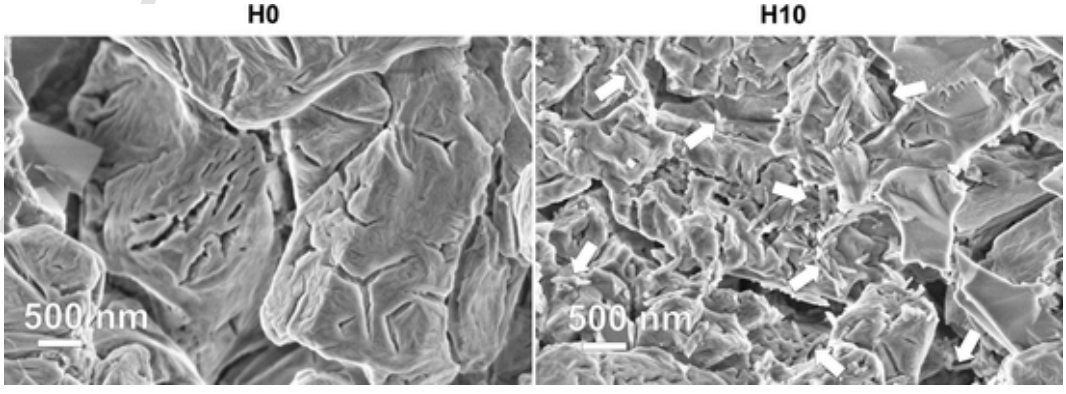

Fig. 3. FE-SEM images of the investigated samples. HNT nanotubes are indicated by the white arrows.

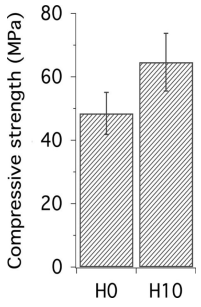

Fig. 4. Results of the compressive strength tests on H0 and *H*10 after 5 days of setting. For each sample, 5 specimens were tested, and the results are reported as average ± standard deviation.

swelling of the nanoclays due to water absorption within its layers. The reinforcing effect observed in MPCs can be mainly ascribed to a filler effect due to HNT's nanotubular morphology which contributes to the formation of a denser matrix by filling the nano-sized porosities. Moreover, HNTs are expected to inhibit the occurrence of cracks' formation thus requiring higher loads to initiate cracking and eventually improving the strength of the composite [66]. It is worth mentioning that although MPC cements are generally appreciated for their high early strength [21], the possibility of further improving their mechanical properties represents an additional bonus when incorporating HNTs as nano-carriers in cementitious matrices.

3.3. Release kinetic

An important feature of HNTs, in addition to their role as reinforcing agents, is the possibility to use them as nano-carriers, since they can load and release active molecules. In the restoration of outdoor cracked structures, the presence of an anti-fouling system in the repair material, to protect the damaged area of the structure from molds and microorganisms, is particularly appealing. For this reason, SA, a well-established antimicrobial agent [45,46], was loaded in the lumen of HNTs nanotubes, and its release both from the nanotubes in water and from the composite MPC/HNTs was studied.

In order to assess the maximum amount of SA that could be released from HNTs, the mass of SA loaded into the nanotubes was quantified by means of thermogravimetric analysis. The TG curves of HNT and HNT-SA, reported in Figure S6 in the Supplementary Material, reveal that SA accounts for 8.7 wt% of the loaded HNTs.

The kinetic of release of SA from HNTs' powder in water shows that the release started immediately after mixing and was complete within about 1 h (see Figure S7). On the other hand, the profile of the release kinetic of SA from HNT/MPC composite (see Fig. 5) is much slower than that of HNT and occurs in about 30 h. Thus, the incorporation of HNT in MPC slows down the SA release from the nanotubes, prolonging its protective effect.

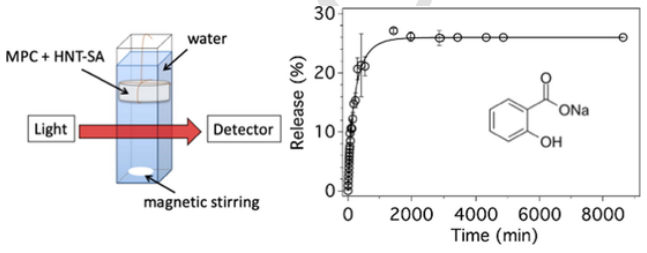

Fig. 5. Schematic representation of the salicylate release from MPC experiments and release kinetic profile of SA from *H*10 composite. Markers represent the average calculated on 3 experimental measurements ± standard deviation; the corresponding fitting curve was calculated according to the Weibull equation.

A quantitative evaluation of the release properties was obtained by fitting the experimental curves according to some of the most commonly used models, as reported in the Materials and Methods section. Korsmeyer-Peppas equation (Eq. (2)) accurately accounts for the release of SA from HNT powders, while the Weibull equation (Eq. (3)) better describes the release of SA from HNT/MPC composite (see Figure S8 and Table S1 for the results of the fittings). As already reported in similar systems, the mechanism controlling the release of SA from HNT is diffusion controlled ($n_{KP} < 0.5$, which corresponds to a Fickian transport in the Korsmeyer-Peppas model) [52–54,67,68]. It was found in the present study that the mechanism ruling the release of SA from HNT/MPC arises from a combination of diffusion and relaxation mechanisms ($0.75 < n_W < 1$, which corresponds to a combination of Fickian diffusion and Case-II transport in the Weibull model [55,56]). These results suggest that the release mechanism of SA is more complex when HNTs are included in the MPC and it could be associated to the migration of SA within the porosities of the cement matrix, which somehow controls the diffusion of SA and slows down the release. It is important to point out that the release profile in a real application would present some differences with the experiment described in this section: in particular, here we observe that after about 30 h of immersion of the whole MPC disk in water the release of SA is complete. When used to fill a crack, only a small part of the surface of the cement would be exposed and, more importantly, it would not be fully immersed in water, but rather in contact with intermittent rain or humidity. Therefore, we can reasonably assume that in a real application the whole release of SA would be far from being complete after 30 h, providing a long-lasting protective effect.

In order to obtain information about the extent of their dissolution in contact with water (see section 2.2.9), MPCs were freeze-dried and weighted. The weight loss is (2.7 ± 0.8) %, demonstrating their excellent resistance to dissolution.

3.4. Application of MPC/HNT composite in cracks

According to the previous results, MPCs are regarded as promising candidates for cracks repair because of their good cohesion, short setting time and final mechanical properties [23,24,69]. The material that we developed presents several advantages with respect to pristine MPCs, as the inclusion of HNTs improves the handling properties, the final compressive strength of the composite and allows for the possibility of including protective molecules to be released when the material gets in contact with water (for instance, due to rain or humidity).

The new MPC composite was tested in a real case-study; some cracks were selected and filled with the *H*10 formulation, following the procedure described in section 2.3 (see Fig. 6). For this preliminary in situ evaluation, an outdoor structure made of concrete, constantly exposed to external environmental agents, was selected. As it is shown in Fig. 6B, the paste can be easily applied with a syringe after 3 min from the beginning of the mixing and can fill the entire depth of the crack, without leaving void space which could eventually cause further cracking. After crack filling, the formulation can also be finely adjusted with a spatula within some minutes from the application, before the final setting time is achieved (*i.e.,* about 14 min). It is worth mentioning that in order prolong the setting time of MPCs and thus to extend the time frame of application, retarders can be incorporated in the formulation [35,57]. The application was monitored for several months, demonstrating excellent stability, as no degradation of the MPC could be observed (see Fig. 6C and 6D). This is in agreement with the results obtained from the resistance to dissolution test, where MPCs lost only 2.7% of their initial weight even after one week of complete immersion in water, suggesting that, even under rainy conditions, these formulations could display a long-lasting stability.

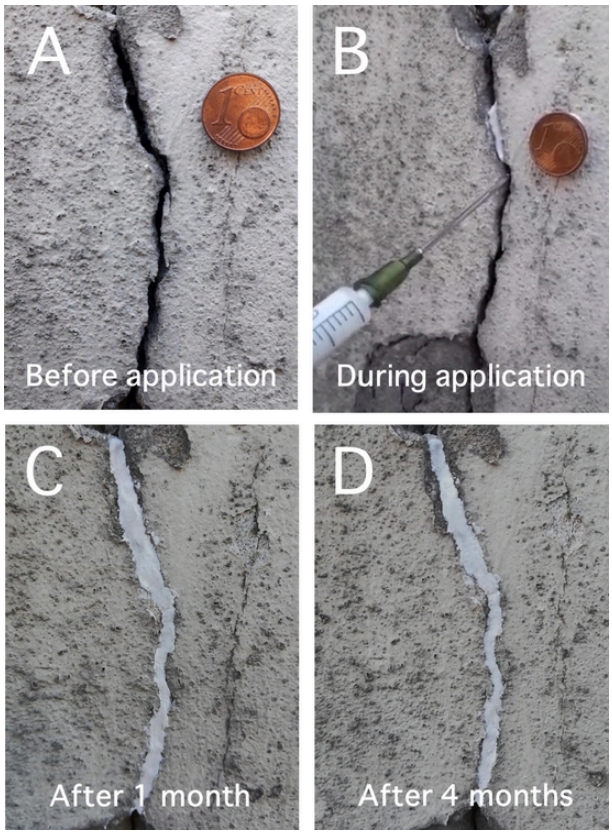

Fig. 6. Pictures of formulation *H*10 in preliminary in-situ applications. Pictures were taken before the application (A), during the application (B), 1 month after the application (C) and 4 months after the application (D). The coin, used on purpose to give an idea of the crack size, has a diameter of 16 mm.

4. Conclusions

MPCs are emerging materials for the repair of damaged structures given their appealing properties such as rapid setting and high early strength. This paper describes an innovative material for crack repair based on a magnesium phosphate cement containing halloysite nanotubes, which improve the mechanical properties and act as nano-carriers to load and release an anti-fouling molecule, *i.e.,* salicylate. It was demonstrated that the inclusion of HNTs in MPCs provides several advantages:

- HNTs improve the consistency and the handling properties of the paste without affecting the setting time, which is important as the quick setting and hardening process of MPCs is commonly regarded as one of their main strengths for repair applications.
- HNTs can be dispersed in the inorganic cement matrix, leading to an improvement of MPCs' compressive strength.
- HNTs can be used to obtain a prolonged release of an anti-fouling molecule from the cement matrix when in contact with water.
- In-situ application by using the cement paste containing HNTs nanotubes to repair a crack shows an excellent injectability and a long-lasting stability.

In conclusion, the results presented in this work show that the inclusion of HNT nanotubes in MPC-based formulations produces several improvements over the available materials and paves the way for the use of clay-based nano-fillers in magnesium phosphate cements for repair applications, especially in the conservation of cement monuments.

CRediT authorship contribution statement

Monica Tonelli: Conceptualization, Data curation, Formal analysis, Investigation, Methodology, Writing - original draft, Writing - review & editing. **Rita Gelli:** Conceptualization, Data curation, Formal analysis, Investigation, Methodology, Writing - original draft, Writing - review & editing. **Francesca Ridi:** Conceptualization, Methodology, Funding acquisition, Resources, Supervision, Validation, Writing - review & editing. **Piero Baglioni:** Funding acquisition, Project administration, Resources, Supervision, Validation, Writing - review & editing.

Declaration of Competing Interest

The authors declare that they have no known competing financial interests or personal relationships that could have appeared to influence the work reported in this paper.

Acknowledgements

This research was funded by H2020, InnovaConcrete Project, grant Agreement number 760858. The CSGI Consortium and MIUR-Italy ("Progetto Dipartimenti di Eccellenza 2018-2022" allocated to Department of Chemistry "Ugo Schiff") are gratefully acknowledged for financial support. Enzo Barlacchi from the "Laboratorio Prove Strutture e Materiali" of the Department of Civil and Environmental Engineering (DICEA), University of Florence, is acknowledged for the compressive strength measurements.

Appendix A. Supplementary data

Supplementary data to this article can be found online at https://doi.org/10.1016/j.conbuildmat.2021.124056.

References

[1] P. Hewlett, M. Liska, Lea's Chemistry of Cement and Concrete, 4th edition, Butterworth-Heinemann, 1998.
[2] L. Bertolini, M. Carsana, M. Gastaldi, F. Lollini, E. Redaelli, Corrosion assessment and restoration strategies of reinforced concrete buildings of the cultural heritage, Mater. Corros. 62 (2) (2011) 146–154, doi:10.1002/maco.201005773.
[3] A. Custance-Baker, G. Crevello, S. Macdonald, K.C. Normandin, Getty Conservation Institute, Conserving concrete heritage: an annotated bibliography, 2015.
[4] M.M. Al-Zahrani, M. Maslehuddin, S.U. Al-Dulaijan, M. Ibrahim, Mechanical properties and durability characteristics of polymer- and cement-based repair materials, Cem. Concr. Compos. 25 (4–5) (2003) 527–537, doi:10.1016/S0958-9465(02)00092-6.
[5] M. Tonelli, P. Baglioni, F. Ridi, Halloysite Nanotubes as Nano-Carriers of Corrosion Inhibitors in Cement Formulations, Materials. 13 (2020) 3150, doi:10.3390/ma13143150.
[6] J.H. Ideker, K.L. Scrivener, H. Fryda, B. Touzo, 12 - Calcium Aluminate Cements, in: P.C. Hewlett, M. Liska (Eds.), Leas Chem. Cem. Concr. Fifth Ed., Butterworth-Heinemann, 2019: pp. 537–584. https://doi.org/10.1016/B978-0-08-100773-0.00012-5.
[7] L. Coppola, D. Coffetti, E. Crotti, Pre-packed alkali activated cement-free mortars for repair of existing masonry buildings and concrete structures, Constr. Build. Mater. 173 (2018) 111–117, doi:10.1016/j.conbuildmat.2018.04.034.
[8] W. Tahri, B. Samet, F. Pacheco-Torgal, J. Aguiar, S. Baklouti, 12 - Geopolymeric repair mortars based on a low reactive clay, in: F. Pacheco-Torgal, R.E. Melchers, X. Shi, N.D. Belie, K.V. Tittelboom, A. Sáez (Eds.), Eco-Effic. Repair Rehabil. Concr. Infrastruct., Woodhead Publishing, 2018: pp. 293–313. https://doi.org/10.1016/B978-0-08-102181-1.00012-5.
[9] A. Van grieken, 16 - Maintenance of aged land-based structures, in: J.K. Paik, R.E. Melchers (Eds.), Cond. Assess. Aged Struct., Woodhead Publishing, 2008: pp. 459–486. https://doi.org/10.1533/9781845695217.5.459.
[10] V. Ducman, S. Kramar, A. Šajna, 11 - Alkali activated repair mortars based on different precursors, in: F. Pacheco-Torgal, R.E. Melchers, X. Shi, N.D. Belie, K.V. Tittelboom, A. Sáez (Eds.), Eco-Effic. Repair Rehabil. Concr. Infrastruct., Woodhead Publishing, 2018: pp. 263–292. https://doi.org/10.1016/B978-0-08-102181-1.00011-3.
[11] F. Pacheco-Torgal, J. Barroso de Aguiar, Y. Ding, W. Tahri, S. Baklouti, 23 - Performance of alkali-activated mortars for the repair and strengthening of OPC concrete, in: F. Pacheco-Torgal, J.A. Labrincha, C. Leonelli, A. Palomo, P. Chindaprasirt (Eds.), Handb. Alkali-Act. Cem. Mortars Concr., Woodhead Publishing, Oxford, 2015: pp. 627–641. https://doi.org/10.1533/9781782422884.4.627.
[12] A. Arora, B. Singh, P. Kaur, Novel material i.e. magnesium phosphate cement (MPC) as repairing material in roads and buildings, Mater. Today Proc. 17 (2019) 70–76, doi:10.1016/j.matpr.2019.06.402.

[13] J.W. Park, K.H. Kim, K.Y. Ann, Fundamental Properties of Magnesium Phosphate Cement Mortar for Rapid Repair of Concrete, Adv. Mater. Sci. Eng. 2016 (2016) 1–7, doi:10.1155/2016/7179403.
[14] F. Qiao, C.K. Chau, Z. Li, Property evaluation of magnesium phosphate cement mortar as patch repair material, Constr. Build. Mater. 24 (5) (2010) 695–700, doi:10.1016/j.conbuildmat.2009.10.039.
[15] B. Jin, L. Chen, B. Chen, Factors assessment of a repair material for brick masonry loaded cracks using magnesium phosphate cement, Constr. Build. Mater. 252 (2020) 119098, doi:10.1016/j.conbuildmat.2020.119098.
[16] S.A. Walling, J.L. Provis, Magnesia-Based Cements: A Journey of 150 Years, and Cements for the Future?, Chem. Rev. 116 (7) (2016) 4170–4204, doi:10.1021/acs.chemrev.5b00463.
[17] C. Moseke, V. Saratsis, U. Gbureck, Injectability and mechanical properties of magnesium phosphate cements, J. Mater. Sci. Mater. Med. 22 (12) (2011) 2591–2598, doi:10.1007/s10856-011-4442-0.
[18] N. Ostrowski, V. Sharma, A. Roy, P.N. Kumta, Systematic Assessment of Synthesized Tri-magnesium Phosphate Powders (Amorphous, Semi-crystalline and Crystalline) and Cements for Ceramic Bone Cement Applications, J. Mater. Sci. Technol. 31 (5) (2015) 437–444, doi:10.1016/j.jmst.2014.12.002.
[19] Z. Ding, Z. Li, Effect of aggregates and water contents on the properties of magnesium phospho-silicate cement, Cem. Concr. Compos. 27 (1) (2005) 11–18, doi:10.1016/j.cemconcomp.2004.03.003.
[20] N. Ostrowski, A. Roy, P.N. Kumta, Magnesium Phosphate Cement Systems for Hard Tissue Applications: A Review, ACS Biomater. Sci. Eng. 2 (7) (2016) 1067–1083, doi:10.1021/acsbiomaterials.6b00056.
[21] Y. Li, B. Chen, Factors that affect the properties of magnesium phosphate cement, Constr. Build. Mater. 47 (2013) 977–983, doi:10.1016/j.conbuildmat.2013.05.103.
[22] S.S. Seehra, S. Gupta, S. Kumar, Rapid setting magnesium phosphate cement for quick repair of concrete pavements — characterisation and durability aspects, Cem. Concr. Res. 23 (2) (1993) 254–266, doi:10.1016/0008-8846(93)90090-V.
[23] F. Qiao, C.K. Chau, Z. Li, Setting and strength development of magnesium phosphate cement paste, Adv. Cem. Res. 21 (4) (2009) 175–180, doi:10.1680/adcr.9.00003.
[24] Q. Yang, B. Zhu, X. Wu, Characteristics and durability test of magnesium phosphate cement-based material for rapid repair of concrete, Mater. Struct. 33 (4) (2000) 229–234, doi:10.1007/BF02479332.
[25] Q. Yang, S. Zhang, X. Wu, Deicer-scaling resistance of phosphate cement-based binder for rapid repair of concrete, Cem. Concr. Res. 32 (1) (2002) 165–168, doi:10.1016/S0008-8846(01)00651-2.
[26] Y. Fang, P. Cui, Z. Ding, J.-X. Zhu, Properties of a magnesium phosphate cement-based fire-retardant coating containing glass fiber or glass fiber powder, Constr. Build. Mater. 162 (2018) 553–560, doi:10.1016/j.conbuildmat.2017.12.059.
[27] N. Yang, C. Shi, J. Yang, Y. Chang, Research Progresses in Magnesium Phosphate Cement-Based Materials, J. Mater. Civ. Eng. 26 (10) (2014) 04014071, doi:10.1061/(ASCE)MT.1943-5533.0000971.
[28] N. Farzadnia, A.A. Abang Ali, R. Demirboga, M.P. Anwar, Effect of halloysite nanoclay on mechanical properties, thermal behavior and microstructure of cement mortars, Cem. Concr. Res. 48 (2013) 97–104, doi:10.1016/j.cemconres.2013.03.005.
[29] E. Joussein, S. Petit, J. Churchman, B. Theng, D. Righi, B. Delvaux, Halloysite clay minerals — a review, Clay Miner. 40 (4) (2005) 383–426, doi:10.1180/0009855054040180.
[30] D.G. Shchukin, H. Möhwald, Smart nanocontainers as depot media for feedback active coatings, Chem. Commun. 47 (31) (2011) 8730, doi:10.1039/c1cc13142g.
[31] E. Abdullayev, R. Price, D. Shchukin, Y. Lvov, Halloysite Tubes as Nanocontainers for Anticorrosion Coating with Benzotriazole, ACS Appl. Mater. Interfaces. 1 (7) (2009) 1437–1443, doi:10.1021/am9002028.
[32] E. Abdullayev, Y. Lvov, Halloysite clay nanotubes as a ceramic "skeleton" for functional biopolymer composites with sustained drug release, J. Mater. Chem. B. 1 (23) (2013) 2894, doi:10.1039/c3tb20059k.
[33] D. Rawtani, Y.K. Agrawal, Multifarious applications of halloysite nanotubes: a review, Rev Adv Mater Sci. 30 (2012) 282–295.
[34] S. Allalou, R. Kheribet, A. Benmounah, Effects of calcined halloysite nano-clay on the mechanical properties and microstructure of low-clinker cement mortar, Case Stud. Constr. Mater. 10 (2019) e00213, doi:10.1016/j.cscm.2018.e00213.
[35] M.A. Haque, B. Chen, Research progresses on magnesium phosphate cement: A review, Constr. Build. Mater. 211 (2019) 885–898, doi:10.1016/j.conbuildmat.2019.03.304.
[36] H.u. Feng, L. Li, P.u. Zhang, D. Gao, J. Zhao, L.u. Feng, M.N. Sheikh, Microscopic characteristics of interface transition zone between magnesium phosphate cement and steel fiber, Constr. Build. Mater. 253 (2020) 119179, doi:10.1016/j.conbuildmat.2020.119179.
[37] H.u. Feng, G. Chen, D. Gao, K. Zhao, C. Zhang, Mechanical Properties of Steel Fiber-Reinforced Magnesium Phosphate Cement Mortar, Adv. Civ. Eng. 2018 (2018) 1–11, doi:10.1155/2018/3978318.
[38] J. Qin, J. Qian, Z. Li, C. You, X. Dai, Y. Yue, Y. Fan, Mechanical properties of basalt fiber reinforced magnesium phosphate cement composites, Constr. Build. Mater. 188 (2018) 946–955, doi:10.1016/j.conbuildmat.2018.08.044.
[39] L.i. Jun, J.i. Yong-sheng, J. Cheng, X.u. Zhishan, Improvement and mechanism of the mechanical properties of magnesium ammonium phosphate cement with Chopped fibers, Constr. Build. Mater. 243 (2020) 118262, doi:10.1016/j.conbuildmat.2020.118262.
[40] Z. Jiang, L. Zhang, T. Geng, Y. Lai, W. Zheng, M. Huang, Study on the Compressive Properties of Magnesium Phosphate Cement Mixing with Eco-Friendly Coir Fiber Considering Fiber Length, Materials. 13 (2020) 3194, doi:10.3390/ma13143194.
[41] X. Man, M. Aminul Haque, B. Chen, Engineering properties and microstructure analysis of magnesium phosphate cement mortar containing bentonite clay, Constr. Build. Mater. 227 (2019) 116656, doi:10.1016/j.conbuildmat.2019.08.037.
[42] X. Lu, B. Chen, Experimental study of magnesium phosphate cements modified by metakaolin, Constr. Build. Mater. 123 (2016) 719–726, doi:10.1016/j.conbuildmat.2016.07.092.
[43] Y. Li, H. Lin, Experimental study on the effect of different dispersed degrees carbon nanotubes on the modification of magnesium phosphate cement, Constr. Build. Mater. 200 (2019) 240–247, doi:10.1016/j.conbuildmat.2018.12.113.
[44] Y. Du, J. Yang, B. Skariah Thomas, L. Li, H. Li, W. Mohamed Shaban, W. Tung Chong, Tung Chong, Influence of hybrid graphene oxide/carbon nanotubes on the mechanical properties and microstructure of magnesium potassium phosphate cement paste, Constr. Build. Mater. 260 (2020) 120449, doi:10.1016/j.conbuildmat.2020.120449.
[45] L. Ghezzi, A. Spepi, M. Agnolucci, C. Cristani, M. Giovannetti, M.R. Tiné, C. Duce, Kinetics of release and antibacterial activity of salicylic acid loaded into halloysite nanotubes, Appl. Clay Sci. 160 (2018) 88–94, doi:10.1016/j.clay.2017.11.041.
[46] A. Spepi, C. Duce, A. Pedone, D. Presti, J.-G. Rivera, V. Ierardi, M.R. Tiné, Experimental and DFT Characterization of Halloysite Nanotubes Loaded with Salicylic Acid, J. Phys. Chem. C. 120 (47) (2016) 26759–26769, doi:10.1021/acs.jpcc.6b0696410.1021/acs.jpcc.6b06964.s001.
[47] I. Banerjee, R.C. Pangule, R.S. Kane, Antifouling Coatings: Recent Developments in the Design of Surfaces That Prevent Fouling by Proteins, Bacteria, and Marine Organisms, Adv. Mater. 23 (6) (2011) 690–718, doi:10.1002/adma.201001215.
[48] M.J. Mosquera, D.M. de los Santos, T. Rivas, P. Sanmartín, B. Silva, New Nanomaterials for Protecting and Consolidating Stone, J. Nano Res. 8 (2009) 1–12, doi:10.4028/www.scientific.net/JNanoR.810.4028/www.scientific.net/JNanoR.8.1.
[49] M. Tonelli, I. Perini, P. Baglioni, F. Ridi, Halloysites as nano-containers for the preparation of antifouling hybrid composites, submitted.
[50] M.V. Ramlogan, A.A. Rouff, An investigation of the thermal behavior of magnesium ammonium phosphate hexahydrate, J. Therm. Anal. Calorim. 123 (1) (2016) 145–152, doi:10.1007/s10973-015-4860-1.
[51] P. Costa, J.M. Sousa Lobo, Modeling and comparison of dissolution profiles, Eur. J. Pharm. Sci. 13 (2) (2001) 123–133, doi:10.1016/S0928-0987(01)00095-1.
[52] N.A. Peppas, B. Narasimhan, Mathematical models in drug delivery: How modeling has shaped the way we design new drug delivery systems, J. Controlled Release. 190 (2014) 75–81, doi:10.1016/j.jconrel.2014.06.041.
[53] P.L. Ritger, N.A. Peppas, A simple equation for description of solute release II. Fickian and anomalous release from swellable devices, J. Controlled Release. 5 (1) (1987) 37–42, doi:10.1016/0168-3659(87)90035-6.
[54] N.A. Peppas, Analysis of Fickian and non-Fickian drug release from polymers, Pharm. Acta Helv. 60 (1985) 110–111.
[55] K. Kosmidis, P. Argyrakis, P. Macheras, A reappraisal of drug release laws using Monte Carlo simulations: the prevalence of the Weibull function, Pharm. Res. 20 (2003) 988–995, doi:10.1023/a:1024497920145.
[56] V. Papadopoulou, K. Kosmidis, M. Vlachou, P. Macheras, On the use of the Weibull function for the discernment of drug release mechanisms, Int. J. Pharm. 309 (1–2) (2006) 44–50, doi:10.1016/j.ijpharm.2005.10.044.
[57] D.A. Hall, R. Stevens, B. El-Jazairi, The effect of retarders on the microstructure and mechanical properties of magnesia–phosphate cement mortar, Cem. Concr. Res. 31 (3) (2001) 455–465, doi:10.1016/S0008-8846(00)00501-9.
[58] L.P. Ogorodova, Y.D. Gritsenko, M.F. Vigasina, D.A. Kosova, L.V. Melchakova, A.D. Fomina, Natural Magnesium Hydrous Orthophosphates Bobierrite and Kovdorskite: FTIR, Raman, Thermal, and Thermochemical Study, Geochem. Int. 58 (2) (2020) 189–199, doi:10.1134/S0016702920020093.
[59] B. Lothenbach, B. Xu, F. Winnefeld, Thermodynamic data for magnesium (potassium) phosphates, Appl. Geochem. 111 (2019) 104450, doi:10.1016/j.apgeochem.2019.104450.
[60] V. Stefov, B. Šoptrajanov, I. Kuzmanovski, H.D. Lutz, B. Engelen, Infrared and Raman spectra of magnesium ammonium phosphate hexahydrate (struvite) and its isomorphous analogues. III. Spectra of protiated and partially deuterated magnesium ammonium phosphate hexahydrate, J. Mol. Struct. 752 (1–3) (2005) 60–67, doi:10.1016/j.molstruc.2005.05.040.
[61] M.I.H. Bhuiyan, D.S. Mavinic, F.A. Koch, Thermal decomposition of struvite and its phase transition, Chemosphere. 70 (8) (2008) 1347–1356, doi:10.1016/j.chemosphere.2007.09.056.
[62] R.L. Frost, M.L. Weier, K.L. Erickson, Thermal decomposition of struvite, J. Therm. Anal. Calorim. 76 (3) (2004) 1025–1033, doi:10.1023/B:JTAN.0000032287.08535.b3.
[63] R. Gelli, L. Mati, F. Ridi, P. Baglioni, Tuning the properties of magnesium phosphate-based bone cements: Effect of powder to liquid ratio and aqueous solution concentration, Mater. Sci. Eng. C. 95 (2019) 248–255, doi:10.1016/j.msec.2018.10.083.
[64] M. Makaremi, P. Pasbakhsh, G. Cavallaro, G. Lazzara, Y.K. Aw, S.M. Lee, S. Milioto, Effect of Morphology and Size of Halloysite Nanotubes on Functional Pectin Bionanocomposites for Food Packaging Applications, ACS Appl. Mater. Interfaces. 9 (20) (2017) 17476–17488, doi:10.1021/acsami.7b0429710.1021/acsami.7b04297.s001.
[65] H. Li, S.-H. Yu, Q.-Z. Yao, G.-T. Zhou, S.-Q. Fu, Chemical control of struvite scale by a green inhibitor polyaspartic acid, RSC Adv. 5 (111) (2015) 91601–91608, doi:10.1039/C5RA17149K.
[66] Z.S. Metaxa, M.S. Konsta-Gdoutos, S.P. Shah, Carbon Nanofiber-Reinforced Cement-Based Materials, Transportation Research Record. 2142 (1) (2010) 114–118, doi:10.3141/2142-17.

[67] E.G. Bediako, E. Nyankson, D. Dodoo-Arhin, B. Agyei-Tuffour, D. Łukowiec, B. Tomiczek, A. Yaya, J.K. Efavi, Modified halloysite nanoclay as a vehicle for sustained drug delivery, Heliyon. 4 (7) (2018) e00689, doi:10.1016/j.heliyon.2018.e00689.
[68] G. Cavallaro, G. Lazzara, S. Milioto, F. Parisi, V. Evtugyn, E. Rozhina, R. Fakhrullin, Nanohydrogel Formation within the Halloysite Lumen for Triggered and Sustained Release, ACS Appl. Mater. Interfaces. 10 (9) (2018) 8265–8273, doi:10.1021/acsami.7b1936110.1021/acsami.7b19361.s001.
[69] G. Mestres, M.-P. Ginebra, Novel magnesium phosphate cements with high early strength and antibacterial properties, Acta Biomater. 7 (4) (2011) 1853–1861, doi:10.1016/j.actbio.2010.12.008.